Pergamon

Journal of Structural Geology, Vol. 16, No. 9, pp. 1297 to 1313, 1994

0191-8141/94 $07.00+0.00

0191-8141(93) E0020-L

A numerical simulation of fabric development in polycrystalline aggregates with one slip system

Y. ZHANG*

Department of Earth Sciences, Monash University, Clayton, Victoria 3168, Australia

B. E. HOBBS and A. ORD

CSIRO Division of Exploration and Mining, Floreat Park, Private Bag, Wembley, WA 6014, Australia

(*Received* 1 *February* 1993; *accepted in revised form* 12 *November* 1993)

Abstract—Fabric development and grain deformation behaviour in polycrystalline aggregrates involving one slip system have been numerically simulated. The model allows inhomogeneous deformation while still ensuring strain compatibility and overall stress equilibrium. Two types of inhomogeneous deformation occur in deformed polycrystals. Inter-grain strain inhomogeneity results from the contrasting deformability of neighbouring grains, which is dominantly determined by the corresponding initial slip-plane orientation. Intra-grain strain inhomogeneity arises because of the need to achieve strain compatibility across grain boundaries. Grain boundaries are generally the places where strain compromise is reached between neighbouring grains. Various microstructures are developed in deformed polycrystals. The development of kink–subgrain structures, a special type of subgrain observed in this model, is closely controlled by initial lattice orientation. The pattern of preferred orientations of slip planes is sensitive to strain history. In contrast, the preferred orientations of longer axes of deformed grains or passive plates in a deforming ductile medium are always parallel to the bulk extension direction, not showing any relevance to deformation history.

INTRODUCTION

AMONG many different theories proposed to predict the development of lattice preferred orientations in polycrystals, the Taylor–Bishop–Hill (TBH) model (Taylor 1938, Bishop & Hill 1951) seems to be the most popular one. In particular, the application of the model to quartz (Lister *et al.* 1978, Lister & Paterson 1979, Lister & Hobbs 1980) has produced fabrics consistent with some natural patterns (Price 1985). However, a major shortcoming of the TBH model is that it assumes homogeneous deformation and co-existence of five independent slip systems; these assumptions are impossible for deformed real polycrystals. In trying to overcome this deficiency, the relaxed constraints model (Honneff & Mecking 1978, 1981, Kocks & Canova 1981) and the self-consistent model (Molinari *et al.* 1987, Wenk *et al.* 1989a,b, 1991) have been developed. Each model allows a certain degree of inhomogeneous deformation and requires fewer slip systems (<5), but on the other hand, there is some loss in local strain compatibility. Jessell (1988a,b) and Jessell & Lister (1990) have modelled fabric development in recrystallizing aggregates by allowing grain boundaries to migrate, but again adopted the homogeneous strain scheme of the TBH model. Another widely quoted work is the pure geometrical model of Etchecopar (1977) and Etchecopar & Vasseur (1987). This model requires homogeneous strain on the single-crystal scale, and also the formation of gaps and overlaps between neighbouring grains results in strain incompatibility. In contrast to the studies mentioned above, two finite element models by Harren & Asaro (1989) and Tharp (1989), respectively, have achieved both inhomogeneous deformation and strain compatibility. However, because the two models employed specially-arranged (equilateral-triangle and orthogonal, respectively) slip systems, the achieved preferred orientation of slip planes can hardly be compared with those developed in real minerals such as quartz, ice and olivine.

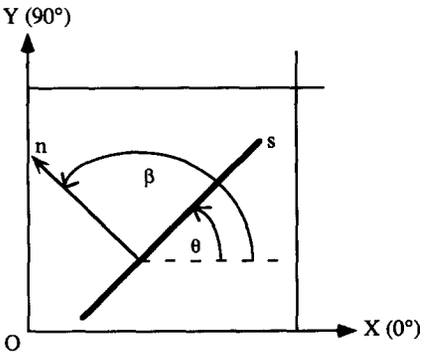

Fig. 1. The definition of the slip system relative to X–Y co-ordinates and a finite difference element. s, slip-plane; n, slip-plane normal; θ and β define the orientation of the slip plane and the slip-plane normal, respectively.

In this paper, we present the results of a one slip-system mechanical model using the computer code FLAC (Fast Lagrangian Analysis of Continua, Cundall & Board 1988). The current model abandons the homogeneous-strain assumption while still maintaining

*Current address: CSIRO Division of Exploration and Mining, Floreat Park, Private Bag, Wembley, WA 6014, Australia.

strain compatibility and dynamic stress equilibrium. The main concerns of the study are the development of lattice preferred orientation, microstructures and grain deformation behaviour; the latter two have been mostly neglected in the previous studies. The one slip-system specification may be a weakness of the model. However, this scheme achieves a unique relationship between the orientation of slip planes and bulk deformation axes. Furthermore, the dominance of one slip system is possible in some minerals (e.g. olivine, ice and quartz deformed under low temperature) (see Nakaya 1954, Nicolas & Poirier 1976).

MODEL DESCRIPTION

FLAC is an explicit, time-marching computer code which, combining the finite difference method, the laws of motion, and the stress–strain constitutive laws of several mechanical models, employs an iterative approach for a series of differential equations to reach the solution. The element matrices of the code are identical to those of a constant-strain finite element, although they are derived by the finite difference method. FLAC has been used for the studies of graben faulting (Cundall 1990), shear band–strain localization (Hobbs & Ord 1989, Cundall 1989, Hobbs *et al.* 1990, Ord 1990) and fabric development in buckle folds (Zhang *et al.* 1993).

The 'Ubiquitous Joint Model' (a constitutive model in FLAC) has been chosen for the simulation of polycrystals. This model treats each grain of a polycrystal as an elastic–perfectly-plastic matrix containing an infinite number of parallel slip planes (one slip system) which also follows elastic–perfectly-plastic behaviour (the critical resolved shear stress law) (see Board 1989, Zhang *et al.* 1993). It needs to be pointed out that the distribution of the slip planes in the matrix is not discrete on the grain scale. There is no way to measure the distance between any pair of slip planes. The existence of the matrix is only shown in that it represents an independent deformation process. The deformation of a polycrystal can be achieved by slip along slip planes or by the deformation of the matrix, or both, depending on the values of the critical resolved shear stress (τ_c) of slip planes and the yield limit (σ_o) of the matrix. In this model, since friction angles for slip planes and the matrix material have both been taken to be zero, τ_c and σ_o are then totally determined by slip-plane cohesion (C_s) and matrix material cohesion (C_m) respectively. By setting

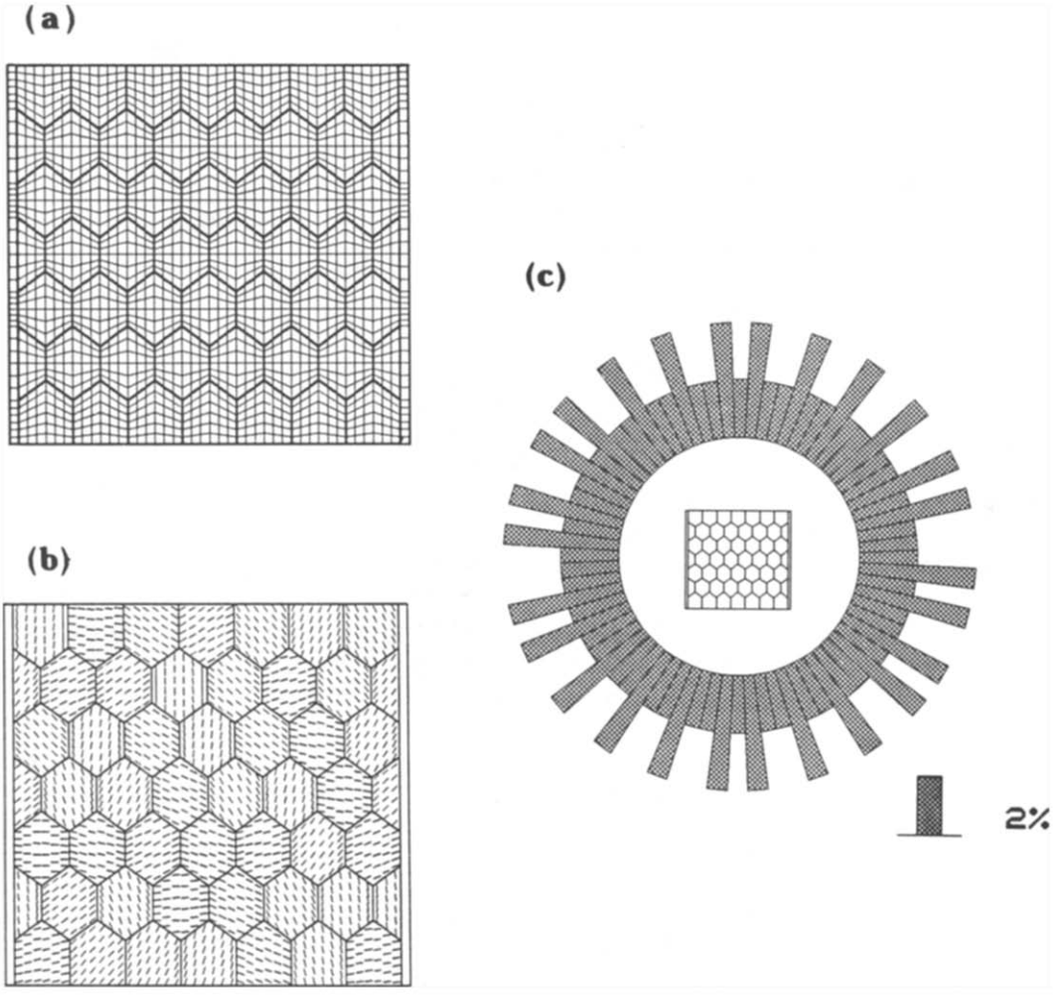

Fig. 2. Specification of the polycrystalline specimen. (a) The finite difference mesh; (b) initial slip-plane traces in the specimen; and (c) the initial orientation distribution of slip-plane normals with respect to the specimen orientation.

Table 1. Material properties

Parameters	Polycrystalline domain		Elastic platens
Density	2467 kg m^{-3}	(Clark 1966)	2650 kg m^{-3}
Shear modulus	4.23×10^{10} Pa	(Clark 1966)	1×10^{11} Pa
Bulk modulus	4.64×10^{11} Pa	(Clark 1966)	1×10^{11} Pa
Matrix cohesion	2×10^{10} Pa		
Matrix friction	0°		
Slip-plane cohesion	2×10^{5} Pa		
Slip-plane friction	0°		
Slip-plane orientation	Variable		

matrix material cohesion much larger than slip-plane cohesion, the yield limit σ_o will be much larger than the critical resolved shear stress τ_c. Therefore, slip on the slip planes will be much easier than flow of the matrix and the domination of slip (dislocation glide) can be ensured (see Zhang *et al.* 1993). To sum up, the current model conforms to the following conditions:

$$\tau_r \leq \tau_c$$

$$\tau_m \leq \sigma_o$$

$$(\sigma_o = C_m) \gg (\tau_c = C_s),$$

where τ_r is resolved shear stress on slip planes and τ_m is the maximum shear stress in the matrix.

A polycrystalline domain is approximated by a two-dimensional mesh comprising quadrilateral elements. Each element can be arbitrarily assigned a slip-plane orientation. This orientation is defined by the counterclockwise-measured angle from the horizontal X-axis to the slip planes (Fig. 1). A crystal grain is a group of neighbouring elements with identical initial slip-plane orientations. Slip-plane rotation takes place as a result of deformation. Misorientation within a single grain is allowed although slip planes within a single element always remain parallel.

NUMERICAL SPECIMEN SET-UP

The mesh chosen for the simulations described here was 44 × 42 in size (Fig. 2a). The two end columns of the mesh were used as stiff platens (the platens were simply abandoned when pure shearing deformation was involved), and that part between the platens, consisting of 1764 elements, was used for the polycrystalline material. Slip-plane orientations were initialized over the mesh (Fig. 2b), creating a numerical polycrystalline specimen containing 49 full hexagonal grains, each composed of 36 elements. The orientation distribution of these slip plane normals is random (Fig. 2c). This configuration was chosen so as to isolate the effect of deformation. For the convenience of describing the position of grains, the expression 'grain (i,j)' is used to identify the grain at the intersection of grain row i and column j in the specimen. The indices i and j are counted from the bottom left corner, so that grain (7,7) denotes the grain at the top right corner of the specimen.

Material properties used in the model are presented in Table 1. The most important parameters are slip-plane cohesion (the critical resolved shear stress) and matrix cohesion (the yield limit), which are chosen as 2×10^5 and 2×10^{10} Pa, respectively. It must be pointed out that neither value represents any real slip system or material. They are chosen just to achieve the domination of slip over the deformation of the matrix. Under this specification, the yielding of the matrix requires a stress of 2×10^{10} Pa and 20% elastic strain (Fig. 3a), whereas slip on slip planes commences at much lower stress (2×10^5 Pa) and strain (0.0002%) (Fig. 3b). This means slip will dominate because stress will be at a level much below the yield stress of the matrix upon the onset of slip. Similarly, large elastic constants for the platens are used in order to obtain high stiffness. The values of the other parameters (density, bulk and shear moduli) are chosen to be those for quartz (Clark 1966).

The deformation of the matrix can be assessed by examining the theoretical maximum shear stresses in the matrix, calculated for grains with various slip-plane orientations at the onset of slip (Fig. 3c). For most grains, the maximum shear stresses in the matrix are obviously well below the yield stress σ_o (2×10^{10} Pa). For those grains with slip planes initially parallel to the principal stress (σ_1 or σ_2), the resolved shear stresses on slip planes are zero and the internal stress in the matrix should be theoretically able to reach σ_o. However, since the matrix will deform elastically as stress increases, slip-plane rotation will immediately occur as the result of deformation and grain interaction. If this slip-plane rotation is larger than 0.001°, slip will start before the stress in the matrix reaches σ_o. Therefore, under the current specification, the matrix material never yields and the small deformation of the matrix is totally elastic.

Specification of boundary conditions involves defining fixed mesh boundaries, and assigning constant displacement rates to certain boundaries. In doing so four deformation histories (axial shortening and extension, pure shearing and simple shearing) are simulated. Total strains are achieved through a series of iterative bulk strain increments.

MODELLING RESULTS

Microstructures

The deformed meshes for the four deformation histories (Fig. 4) show that initially-equiaxed hexagonal grains have mostly become flattened with irregular geometries.

Although the direction of flattening is different for different deformation histories and the degree of flattening varies from grain to grain, a general feature is that the longer axes of deformed grains are roughly parallel to the corresponding bulk extension axis. It can also be seen from the deformed meshes that some local small shear bands have developed. These shear bands mostly occur along grain boundaries, strongly-deformed grains or intragranular strain localization zones.

The spatial distributions of slip-plane traces in deformed specimens are shown in Fig. 5. In many grains (e.g. grains (2,2), (3,7), (1,5) and (2,3) in Figs. 5a, b, c & d, respectively), the current orientations of slip-plane traces demonstrate large intragranular jumps along some lines. These lines divide an original grain into two or more sub-domains which currently show distinct orientations of slip-plane traces (Figs. 6a & b). We consider these lines as subgrain boundaries and these domains as subgrains, since they involve lattice misorientation in host grains (see Fig. 6a). It needs to be mentioned that some subgrains developed in this study have reached quite large misorientations (e.g. grain (2,2) in Fig. 5a), probably indicating the formation of new grains. They are still referred to as subgrains here to emphasize their affiliation with the host grain.

Note that the misorientations of slip-plane traces in some grains (e.g. grains (2,4), (5,2), (1,7) and (6,3) in Figs. 5a, b, c & d, respectively) exhibit kink geometries. This 'lattice' plane kinking also coincides with material line (mesh line) kinking in these grains (see Fig. 4). The subgrains displayed by such a style of slip-plane misorientation are generally characterized by subparallel subgrain boundaries (Fig. 6b). This special category of subgrain can be termed kink–subgrain structure to emphasize its kink-style misorientation.

Inspection of initial slip-plane orientations (see Fig. 2b) reveals that for each deformation history, kink–subgrain structures (Fig. 5) generally develop in those grains with slip-plane orientations initially subparallel to the bulk shortening direction. These are grains with initial slip-plane orientation angles of around 0° in the axial shortening and pure shearing histories (e.g. grains (1,1), (1,7), (2,4) and (5,6) in Figs. 5a & c), 90° in the axial extension history (e.g. grains (5.2), (5,4) and (6,4) in Fig. 5b), and 45° in the simple shearing history (e.g. grains (1,3), (3,6) and (6,3) in Fig. 5d). At these special orientations, slip planes are subjected to large bending moments which nucleate the bending of slip planes. Any initial bending of slip planes can facilitate kinking. This process is believed to be common in crystals with one slip

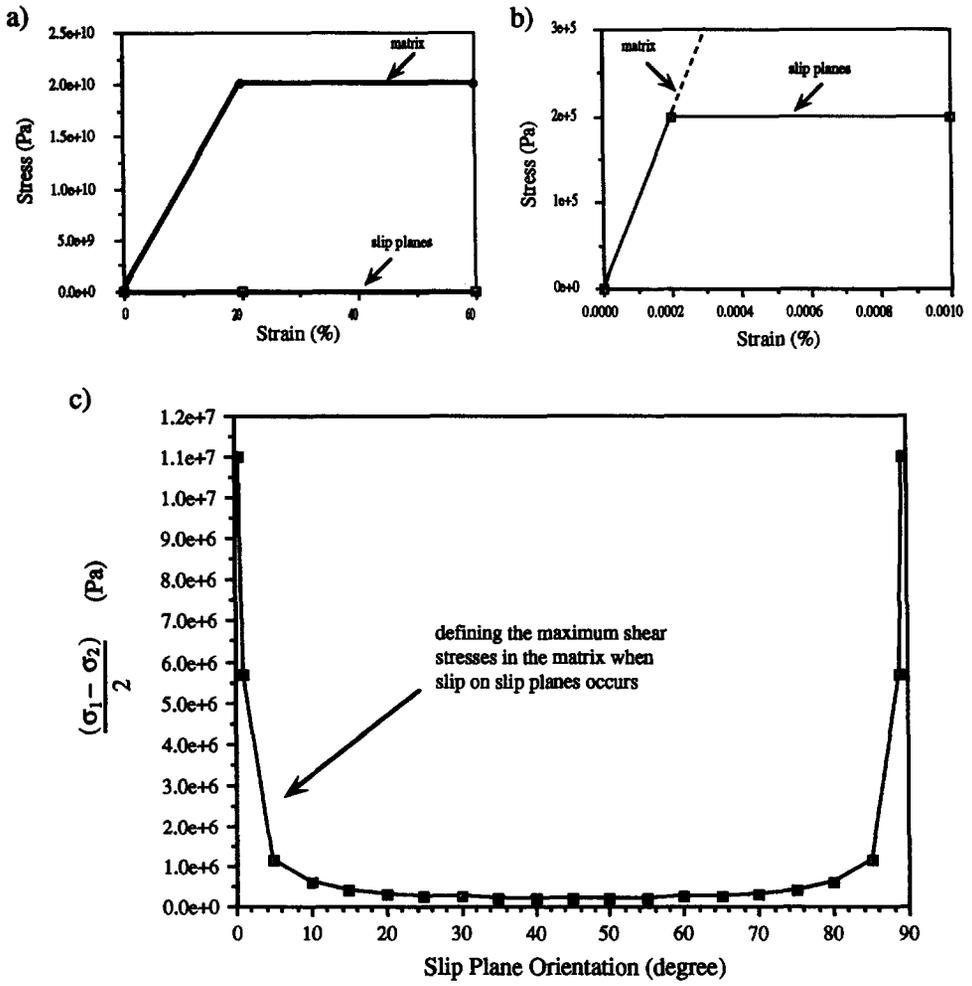

Fig. 3. (a) Theoretical stress–strain curves for the slip planes and the matrix material between the slip planes. (b) Enlarged view of the stress–strain curve for the slip plane. (c) The theoretical maximum shear stress in the matrix for grains with various slip-plane orientations at the onset of slip.

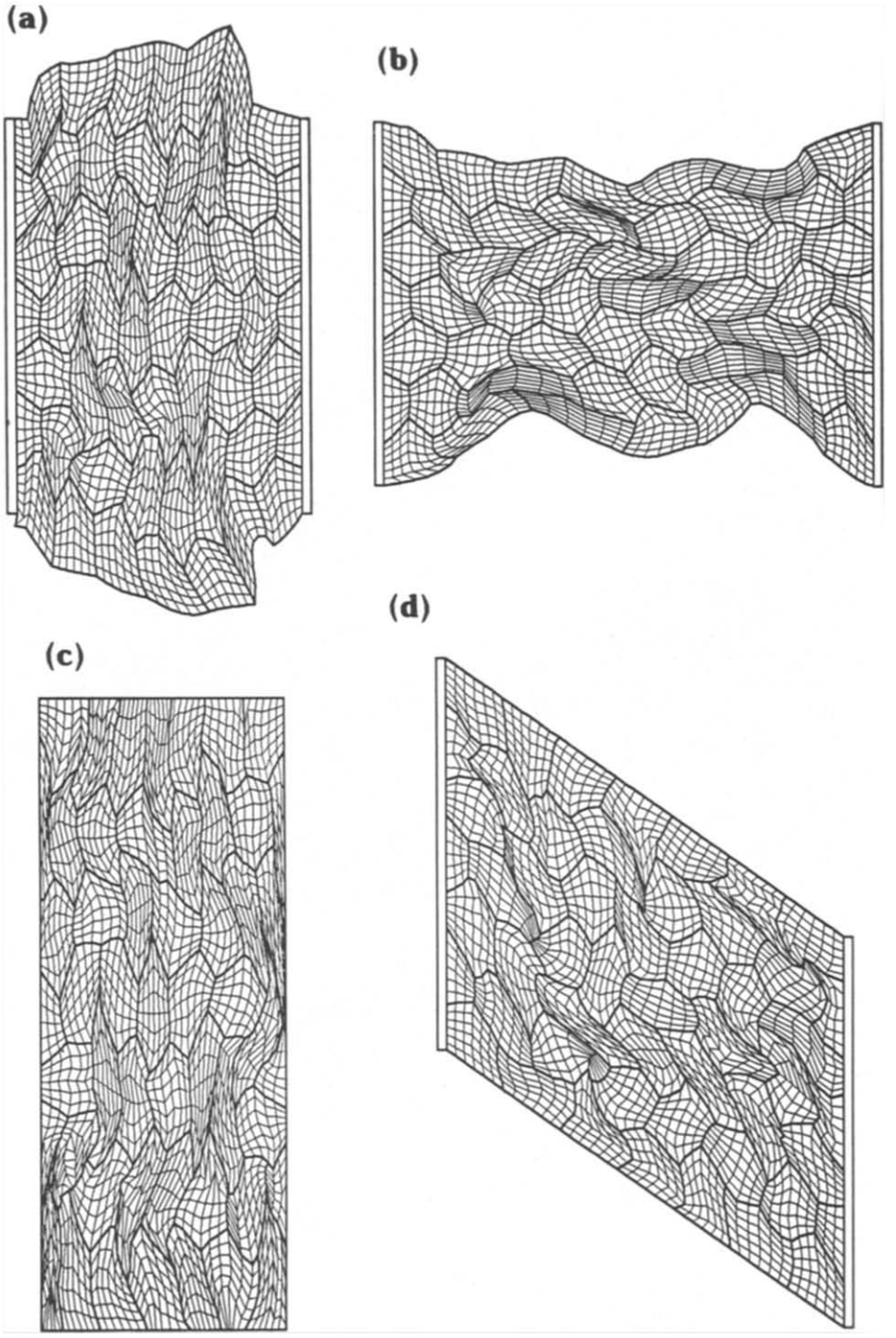

Fig. 4. Deformed finite difference meshes. (a) Axial shortening, 29% bulk shortening; (b) axial extension, 33% bulk extension; (c) pure shearing, 38% bulk shortening; and (d) simple shearing, $\gamma = 0.72$.

system (Nicolas & Poirier 1976). Subgrain formation through the operation of kinking has also been observed in experimentally deformed octachloropropane (Means & Ree 1988).

The development of kink–subgrain structures, is, therefore, the result of application of principal stresses in a special orientation with respect to initial slip planes. This can be considered as an important subgrain-formation mechanism. In contrast, the other subgrains (e.g. grain (2,3) in Fig. 5d) are caused dominantly by neighbouring grain interaction. Grain interaction is a mechanism extensively operative in inhomogeneously-deformed polycrystals. This mechanism leads to large variations of the deformation field within single grains, particularly near grain boundaries; subgrains develop as a result of this variation.

In contrast to sharp variations in slip-plane orientation in the case of subgrains, slip-plane misorientation in some grains is gentle and progressive (Fig. 6c; also see grain (1,4) in Fig. 5a and grain (6,3) in Fig. 5c). These undulatory lattice orientations correspond to the geological phenomenon of undulatory extinction.

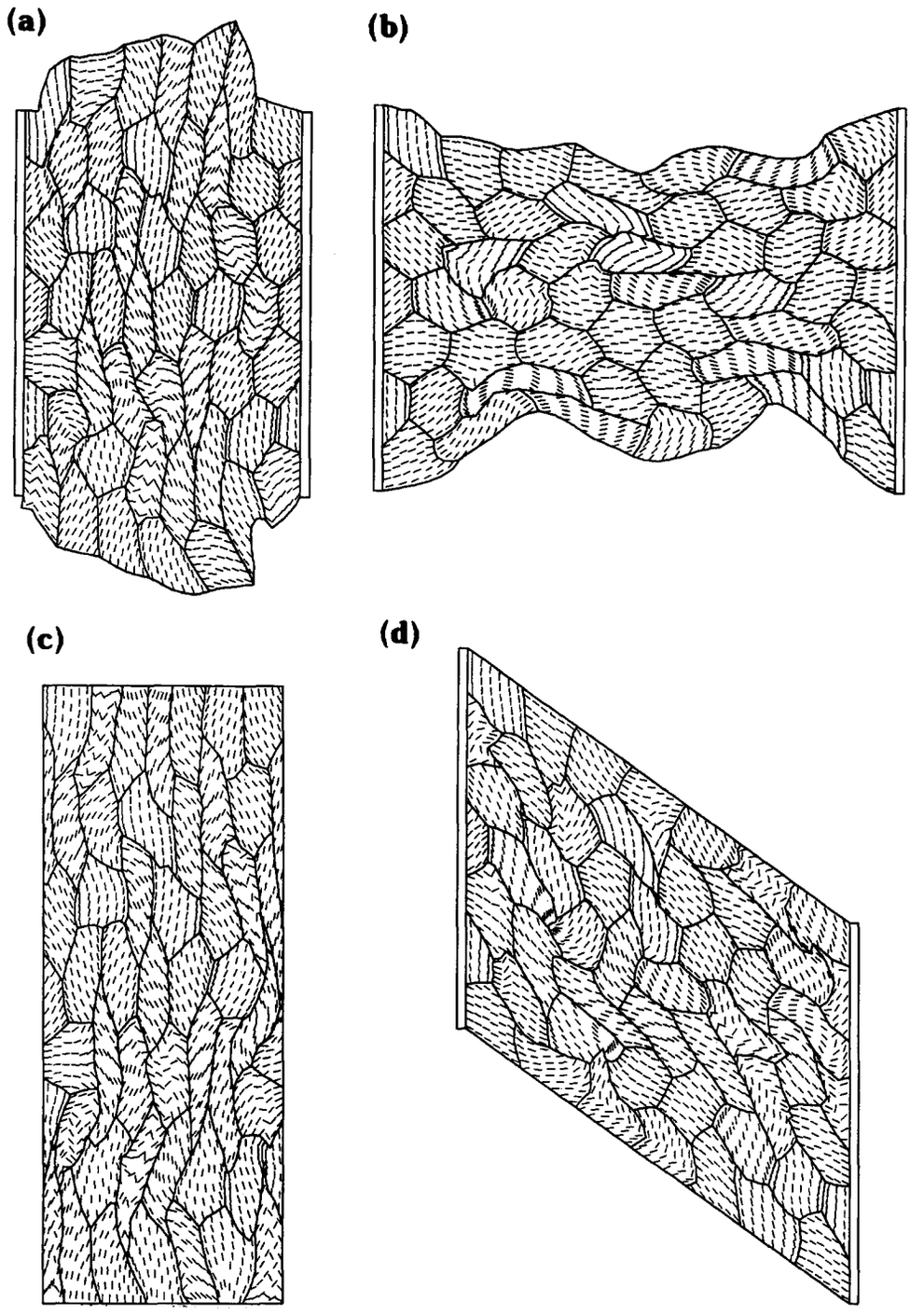

Fig. 5. Final spatial distribution of slip-plane traces. See Fig. 4 for explanation of (a), (b), (c) and (d).

Preferred orientations

The final orientation distribution of slip-plane normals is given in Fig. 7 (left column), showing that different lattice preferred orientations develop for different deformation histories.

Axial shortening (29% *bulk shortening*). Two maxima of slip-plane normals develop approximately symmetrically about the bulk shortening direction (Fig. 7a, left column). The included angle between the two maxima is about 50°.

Axial extension (33% *bulk extension*). A single maximum of slip-plane normals develops normal to the bulk extension direction (Fig. 7b, left column). A small peak is also observed roughly parallel to the bulk extension direction. This is caused by the grains adjoining the platens and having initial slip planes roughly normal to the bulk extension direction (platen effect).

Pure shearing (38% *bulk shortening*). The final distribution of slip-plane normals shows two maxima symmetrical about the bulk shortening direction (Fig. 7c, left column). The included angle between the two maxima is 30°, much smaller than that for axial shortening.

Simple shearing ($\gamma = 0.72$). Two maxima can be distinguished (Fig. 7d, left column). The first is approximately normal to the shearing plane, indicating a pre-

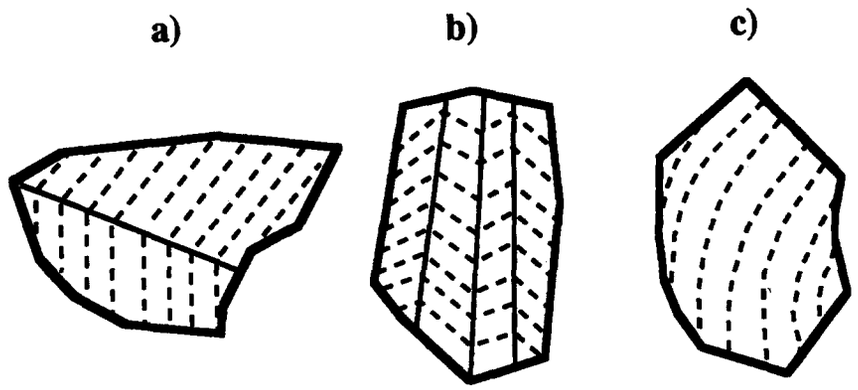

Fig. 6. Three types of slip-plane misorientation developed in this model. (a) The subgrain type; (b) the kink–subgrain type; and (c) the undulatory lattice orientation type.

ferred alignment of slip planes along the shearing plane. The second is a broad maximum approximately symmetrical to the first about the bulk finite shortening direction, representing a group of concentrated slip planes oblique to the shearing plane.

In each of the above deformation histories, the preferred orientation of slip-plane normals strengthens as bulk deformation increases. This can be illustrated by the fabric patterns for three consecutive stages of the pure shearing history (Fig. 8). The preferred orientation is quite weak at 9% bulk shortening and is relatively intense by the 19% stage. Then by the 38% stage a clear two-maxima pattern has developed. This fabric transition also shows that slip-plane normals generally rotate toward the bulk shortening axis, although the maxima of slip-plane normals do not lie in this direction.

Because the fabrics described above are all achieved from a particular grain combination or slip-plane orientation combination (Fig. 2b), a question may be asked if this particular combination has any influence on the final fabric. To investigate this influence, we have performed another pure shearing simulation, which starts from a different grain combination (Fig. 9) but the same lattice orientation distribution pattern (see Fig. 2c). The final orientation distribution of slip-plane normals (Fig. 9) again shows two maxima symmetrical about the bulk shortening axis with an included angle of 35°, basically similar to the previous pattern (Fig. 7c, left column). This demonstrates that the starting grain combination does not influence the final fabric pattern as long as the initial orientation distribution remains random.

It is noted that the preferred orientations of slip-plane normals for axial shortening and pure shearing histories do not coincide with the bulk shortening direction, even though the concentration of slip-plane normals in this direction (Figs. 7a, & c, left column) is significantly greater than in the starting distribution (Fig. 2c). Instead, the fabrics for these two histories are both characterized by two maxima symmetrically disposed about the bulk shortening direction. This pattern can be considered typical of compressional deformation because the two histories both feature continuous shortening in the horizontal direction.

The orientation distribution of the long axes of flattened grains in deformed specimens can be illustrated by grain shape fabrics (Fig. 7, right column). For axial shortening, pure shearing and simple shearing histories, grain shape fabrics all show a single maximum parallel to the bulk finite extension direction. For axial extension, the peaks of the grain shape fabrics are situated within 20° of the bulk extension direction. Obviously, the preferred orientations of long axes of deformed grains differ from lattice preferred orientations.

Deformation features

Strain distributions are clearly inhomogeneous for all the deformation histories (Fig. 10). Some grains are strongly deformed, such as grains (3,2) and (5,3) in Fig. 10(a), (1,3) and (2,6) in Fig. 10(b), (1,1) and (3,2) in Fig. 10(c) and (3,3) and (5,7) in Fig. 10(d), whilst other grains are deformed much more weakly, such as grains (2,3) and (5,2) in Fig. 10(a), (2,4) and (7,2) in Fig. 10(b), (5,2) and (4,6) in Fig. 10(c) and (2,5) and (5,5) in Fig. 10(d). A high-strain grain differs from a neighbouring low-strain grain both in strain magnitude and in strain orientation. Strain heterogeneity is observed not only on the inter-grain scale but also on the intra-grain scale. Strain in different parts of a grain can be quite different (e.g. grain (7,1) in Fig. 10a). It should be emphasized that in spite of strain heterogeneity, strain compatibility is still maintained in specimens, as demonstrated by grain boundaries remaining in contact.

Grain interaction can be recognized from the large variations in element distortion (Fig. 4) and strain ellipse axis orientation (Fig. 10) near grain boundaries, particularly between a high-strain grain and a low-strain grain. On the high-strain grain side, strain usually shows a decrease near the boundary, whereas strain shows an increase on the low-strain grain side.

The state of strain in axial deformation histories (Figs. 10a & b) is significantly influenced by the specimen boundaries. Because the undeformable platens on the lateral sides of the specimen have welded contacts with the polycrystalline domains, they have confined the displacement of all the adjoining grains in the Y (vertical) direction. This has impeded the deformation of these grains, which generally show small strains. By

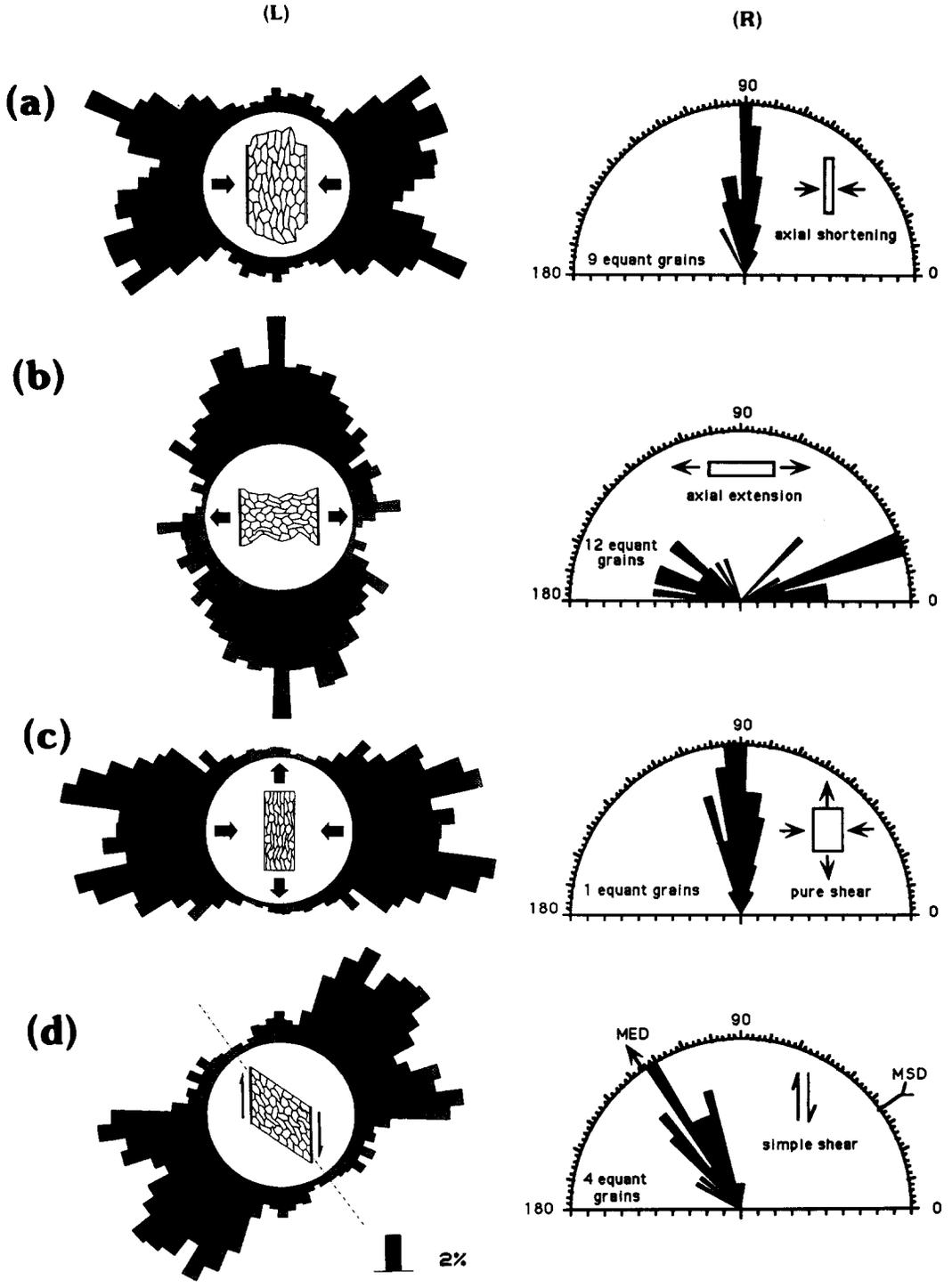

Fig. 7. Final orientation distribution of slip-plane normals with respect to the orientations of deformed specimens (L: left column) and grain shape fabrics showing the orientation distribution of longer axes of deformed grains (R: right column). (a), (b), (c) and (d) correspond to those runs shown in Fig. 5. MED and MSD: maximum finite extension and shortening directions, respectively. The number of equant grains gives the number of those grains not showing evident longer axes after deformation.

contrast, the free boundaries of the specimen under axial deformation are subjected to very weak constraints in the Y direction so that the vertical displacement of the grains in these locations is relatively easy. As a result, the deformed specimens show strong extrusion and necking geometries along these boundaries in axial shortening and axial extension histories, respectively. This generally intensified the deformation of the grains involved.

By comparing the strained state (Fig. 10) with the corresponding initial slip-plane orientations (Fig. 2b), it is found that the deformability of a grain is closely related to its initial slip-plane orientation; the initial slip-plane orientation determines the spatial relationship between the slip planes and the bulk deformation axes. This relation can be illustrated more explicitly by plotting the strain ellipticities of grains against initial slip-plane orientations and bulk strains (Fig. 11). As might

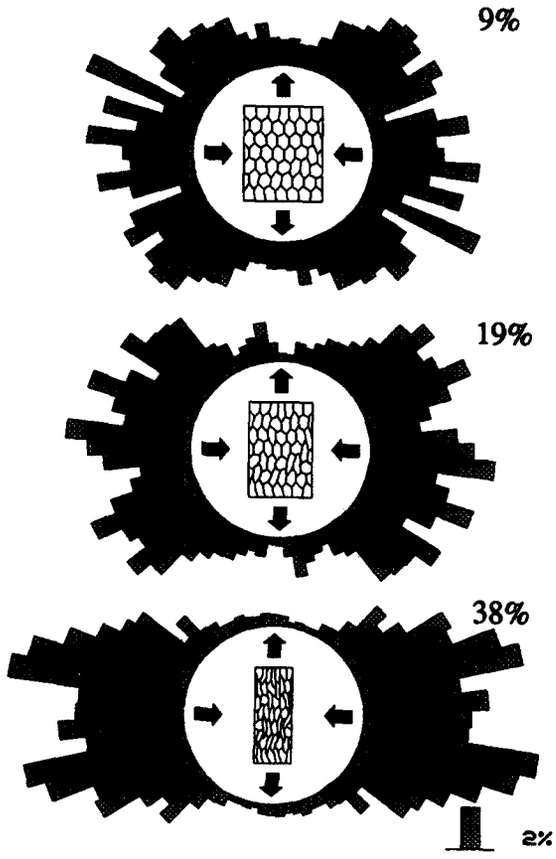

Fig. 8. The slip-plane normal distributions for the three consecutive stages of the pure shearing history; bulk deformations are 9, 19 and 38% shortening, respectively.

be expected, the lowest strains occurred in the grains possessing initial slip-plane orientations approximately normal to the bulk shortening direction. These are grains with slip-plane orientations of about 90° for axial shortening and pure shearing (Figs. 11a & c), 0°/180° for axial extension (Fig. 11b), and 135° for simple shearing (Fig. 11d). At these orientations, slip is most difficult owing to the smallest resolved shear stresses on the slip planes. We can call these grains the 'hard' grains, emphasizing their least deformability. The situation for high-strain grains is more complex because high strain can occur in grains with several different slip-plane orientations for each deformation history. For coaxial deformation histories (Figs. 11a, b & c), the high strain grains are those with slip planes initially parallel to the bulk shortening direction (the 0°/180° direction for axial shortening and pure shearing, and the 90° direction for axial extension), or oblique to this direction at about 30° (the 30° and 150° directions for axial shortening and pure shearing, and the 60° and 120° directions for axial extension). For simple shearing (Fig. 11d), the grains showing high strains are also characterized by three initial slip-plane orientations. They are the orientations close to the bulk shortening direction (the 49° orientation), parallel to the shearing direction (the 90° orientation), and oblique to the bulk shortening direction at about 25° (only true for one of the two positions, that is, the 20° orientation). In contrast to the 'hard' grains, these high-strain grains can be termed the 'soft' grains, emphasizing their high deformability. The observation of 'hard' grains and 'soft' grains has been reported for experimentally deformed octachloropropane (Ree 1990). Furthermore, the coexisting configuration of low-strain 'hard' grains and high-strain 'soft' grains, described here (see Fig. 10), is comparable to the natural observations of undeformed or weakly-deformed quartz grains surrounded by strongly-deformed grains (Tullis *et al.* 1973). This feature is also clearly shown in an experimentally-sheared ice specimen (see Burg *et al.* 1986, fig. 6). A number of hardly deformed ice crystals can be seen to be isolated among strongly deformed–recrystallized grains. In particular, the slip lines of these grains indicate that they all have basal planes roughly normal to the bulk shortening direction of the simple shear, consistent with the current prediction.

Exceptions to the above rules of grain deformability in terms of initial slip-plane orientation could be caused by the local deformation environment around a grain, which involves overall boundary conditions and the deformabilities of neighbouring grains. For example, a grain with a deformation-favourable initial slip plane orientation could exhibit small strain if neighbouring grains or the boundary condition (such as the platen effect) create an unfavourable deformation regime (e.g. grain (3,1) in Fig. 10a and grain (3,7) in Fig. 10c). This type of exception has weakened the fabrics shown in Fig. 11.

Corresponding to inhomogeneous strain, the stress distribution in deformed polycrystalline specimens is also inhomogeneous. This can be clearly seen, for example, from the final stress field for the axial shortening history (Fig. 12). Stresses generally show significant variations or local concentrations at grain boundaries, particularly near triple junctions, where grain interaction occurs and state of strain varies. Low stresses are caused by free mesh boundaries.

DISCUSSION

Preferred orientations

It must be kept in mind that lattice preferred orientation developed in a model is dependent on the slip-system framework. A different spcification, such as two orthogonal slip systems (Tharp 1989) or three slip systems arranged in an equilateral triangle (Harren & Asaro 1989), can lead to quite different results. In the current model, a one slip-system specification does not exactly coincide with any specific type of mineral. However, if we correlate slip planes with basal planes [0001] in quartz or ice, the preferred orientation of slip-plane normals can then be compared with *c*-axis fabrics in these real minerals.

Lattice preferred orientations developed in this model are in good agreement with the patterns developed in deformed ice and peridotites. For coaxial pure shearing (flattening) deformation, the experimental ice *c*-axis

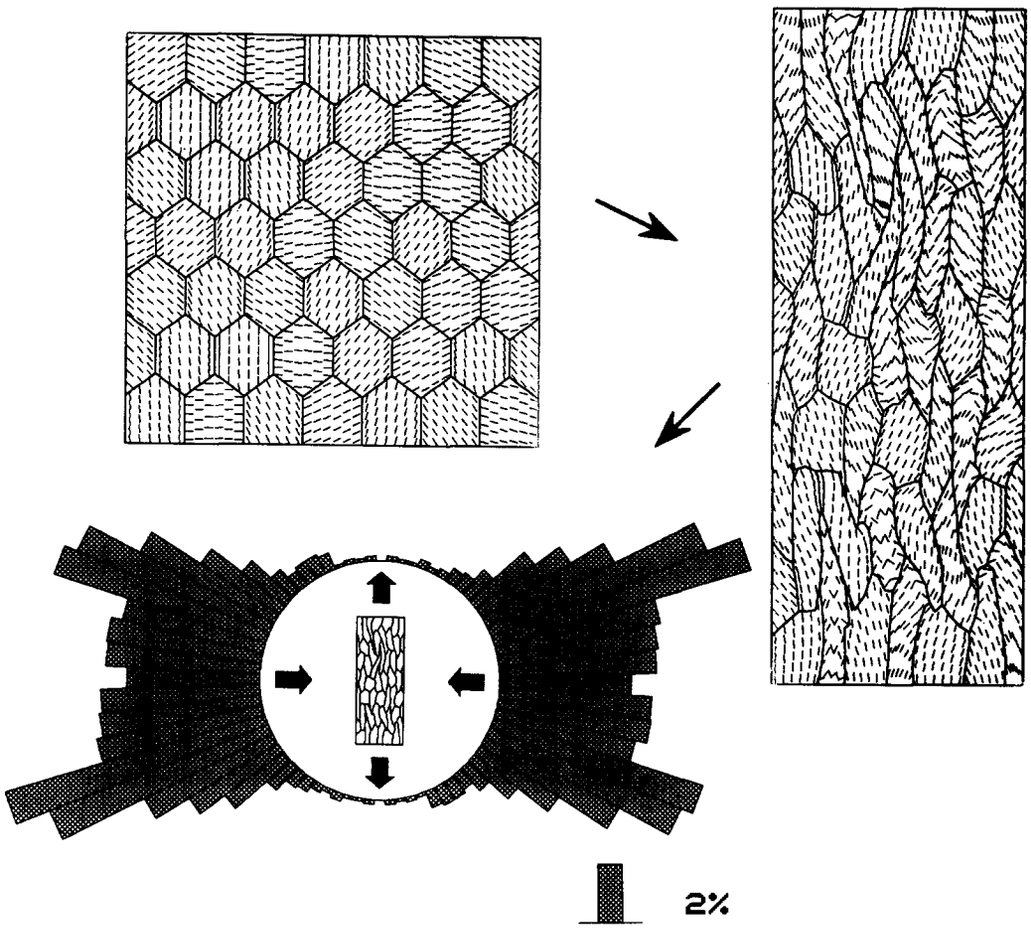

Fig. 9. The initial and final slip-plane traces and the final orientation distribution of slip-plane normals for a pure shearing model starting from a different grain (slip-plane) configuration to that shown in Fig. 2(b).

fabrics obtained by Wilson (1982) display small circles about the shortening axis. The preferred orientations of the [010] axes for experimentally deformed peridotites at 44% shortening, reported by Nicolas *et al.* (1973), are a number of maxima located around the shortening axis. The two-dimensional projection of these fabric patterns just coincides with the two-maxima pattern obtained in this study (Figs. 7a & c, left column). For simple shearing, there is also the excellent consistency between the current pattern (Fig. 7d, left column) and the *c*-axis fabrics of experimentally and naturally deformed ice (Hudleston 1980, Bouchez & Duval 1982) at comparable strain levels. That is, they both show two maxima roughly symmetric about the bulk shortening axis, with one maximum normal to planes of shear. Furthermore, the preferred orientations obtained here are also comparable to the fabric patterns of the Etchecopar model (Etchecopar 1977) and some of the patterns of the TBH models (Lister & Hobbs 1980, Jessell 1988a,b), particularly the first model.

A certain degree of bulk deformation is the prerequisite for the clear development of lattice preferred orientation. Comparing the current model with the Etchecopar (1977) model, we find that for the clear development of fabrics, Etchecopar's model generally needs higher bulk deformation. For example, at the stage of $\gamma = 0.72$, the Etchecopar model did not produce a distinct fabric, whereas a preferred orientation is developed at this stage in the current model. This is possibly because the Echecopar model involves the formation of overlaps and gaps in deformed specimens, which accommodates a certain amount of bulk deformation. For the same bulk deformation, the intra-grain strain and lattice rotation in Etchecopar's model should be less than in this model.

It is often assumed that slip planes are preferably aligned parallel to the bulk extension direction under coaxial flattening, and parallel to the shearing plane in simple shearing. However, Wenk & Christie (1991) argued that this is not true in many situations, such as in polycrystals. The current results show that the final prevalent alignment of slip planes for coaxial flattening histories is symmetrical about the bulk extension direction at 10°–25°. This favours Wenk & Christie's claim, but there is the question as to why this occurs even in polycrystals with one slip system. We believe that the answer lies in the nature of polycrystalline deformation. In a polycrystal, each grain deforms differently from the others because the constituent grains have different lattice orientations. However, the imposed bulk strains must be compatibly accommodated over the polycrystalline domain. Grain interaction then arises and leads to the development of local stress fields that deviate from the bulk frame. That is, the orientations of local princi-

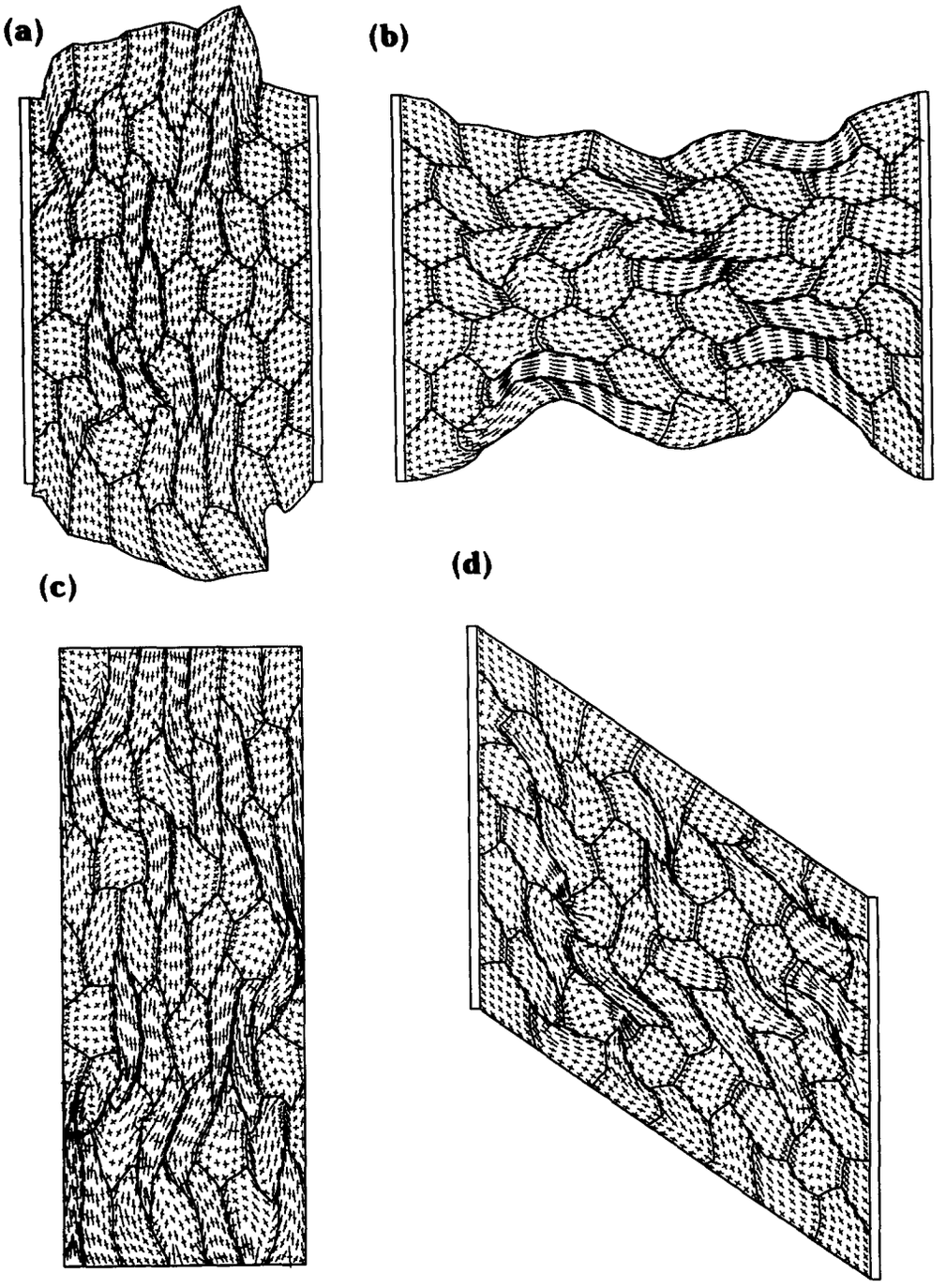

Fig. 10. Distribution of strain ellipse axes in deformed specimens. See Fig. 4 for explanation of (a), (b), (c) and (d).

pal minimum stresses (local extension) generally deviate from the bulk extension direction (see Fig. 12). Statistically, these deviations are symmetrical about the bulk extension direction at a small angle. As deformation proceeds, slip planes rotate generally toward the bulk extension direction but are stabilized when reaching the corresponding local extension direction, so that they can hardly reach the bulk extension direction. As a result, slip planes prevalently orient themselves symmetrically about the bulk extension direction. This interpretation is supported by the fact that final slip-plane traces are approximately parallel to the local extension directions (see Figs. 5a and 12). The situation will be different for single crystals in which bulk and local stress fields are identical. The stable position for slip-plane alignment should always coincide with the bulk extension direction. For simple shearing, the current result, together with those of many other studies (e.g. Etchecopar 1977, Hudleston 1980, Lister & Hobbs 1980, Bouchez & Duval 1982, Burg *et al.* 1986), does not support Wenk & Christie's (1991) suggestion. We find that macroscopic shearing planes are indeed favourable positions for slip-plane alignment. This is probably because, in simple shearing, a frame with slip planes parallel to the shearing plane is more favourable for simple shearing to proceed than any other frame. If slip planes are not initially parallel to the shearing plane, they could rotate toward the shearing plane, whereas if they are initially parallel

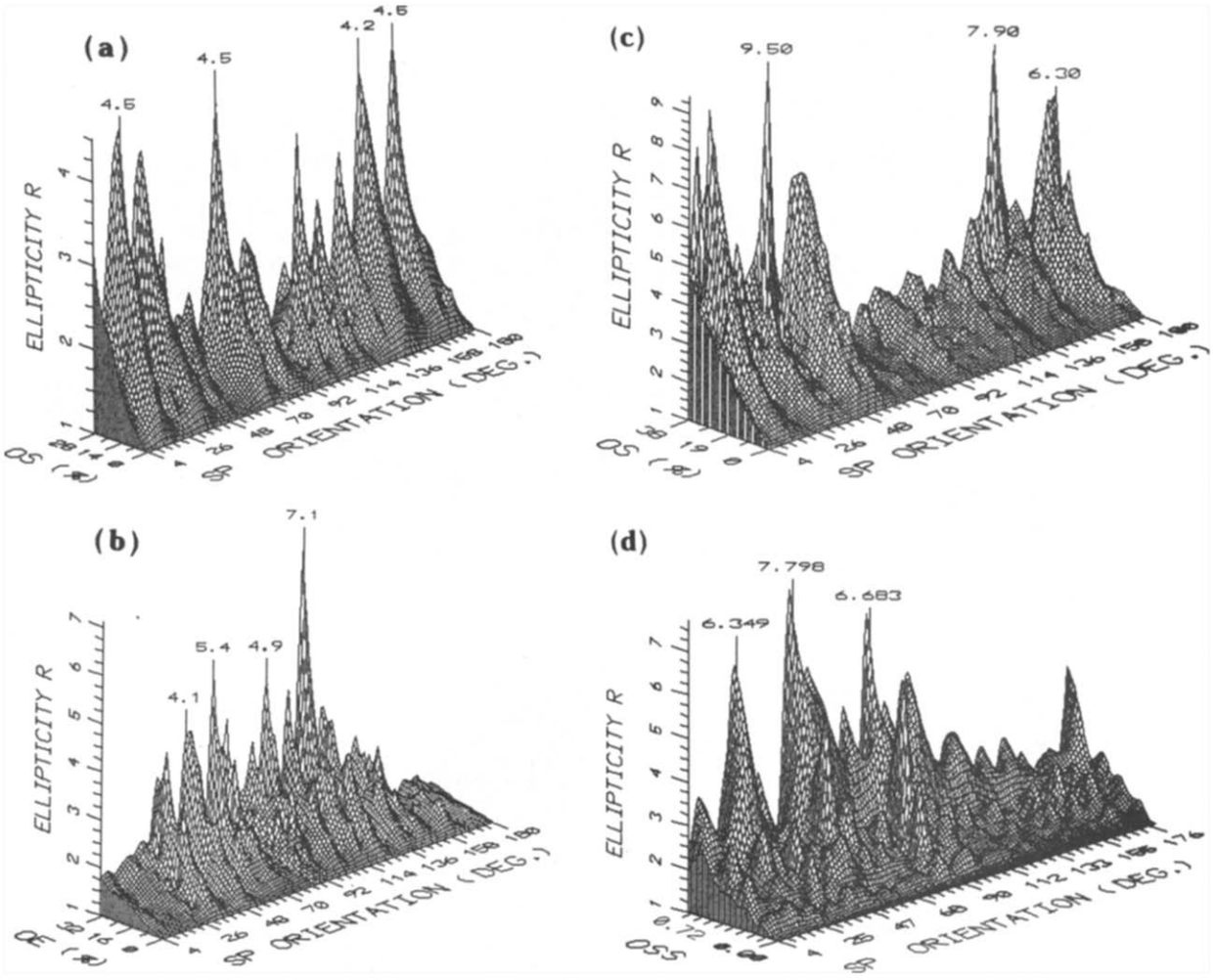

Fig. 11. Presentation of grain-average ellipticity vs initial slip-plane orientation and bulk strain. (a), (b), (c) and (d) correspond to the runs shown in Fig. 4. OS, OE, OSS and SP denote overall shortening, overall extension, overall shear strain and slip plane, respectively.

to the shearing plane, it will be difficult for them to rotate away since this consumes more energy than maintaining the original orientation.

It should be emphasized that stable orientations for slip planes in polycrystals and for passive plates or rods in a ductile medium are different. In the latter situation, the passive rotation of plates or rods, which have no role in accommodating the applied bulk deformation, is actually driven by the deformation of the homogeneous medium material. We have modelled this case using a slip-plane cohesion (2×10^{14} Pa) much larger than matrix cohesion (2×10^{9} Pa); the other specifications remain the same (see Fig. 2). In this situation, the imposed bulk strains are totally accommodated by plastic flow in the matrix material, and slip planes only act as passive markers. The results (Fig. 13) show that the preferred orientations of 'slip-plane' normals for pure shearing and simple shearing histories are parallel to the maximum finite flattening direction in both cases, and obviously different from the fabric results for polycrystals under the corresponding deformation history (Figs. 7c & d, left column).

A weakness of the current model is that the bulk strains attained are generally low due to the geometrical problems of computation. the bulk strains achieved for coaxial deformation histories are less than 40% shortening, a critical threshold proposed by Tharp (1989) for sharply enhancing preferred orientations. Shear strain for simple shearing (0.72) is also less than 1. This may limit the extrapolation of the current fabric results to higher deformation levels. At a sufficiently high shear strain, for example, the fabric of simple shearing may lose its symmetry and slip planes may become parallel to shearing planes.

Microstructures

Jessell (1988a,b) has simulated subgrain formation at grain boundaries, but excluded intragranular subgrains. In contrast, the subgrains developed in this model mostly belong to the intragranular category. In most situations, a group of subgrains develops over a whole host grain or in part of a host grain, similar to what occurs in some grains of experimentally deformed ice (Burg *et al.* 1986) and octachloropropane (Means & Ree 1988).

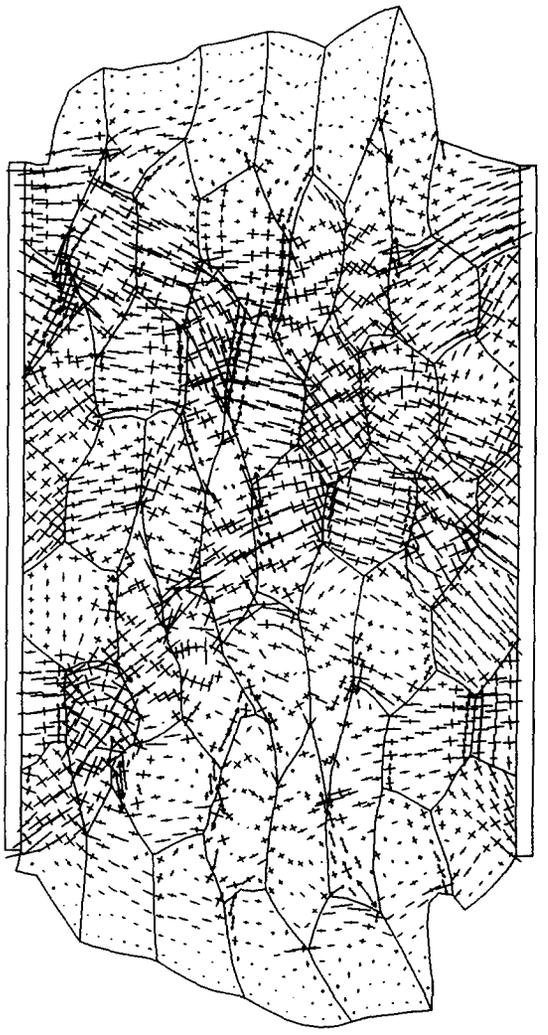

Fig. 12. Principal stress distribution in the deformed specimen for the axial shortening history.

Kink–subgrain structures are a special type of subgrain developed in this model, which mostly fall into the fixed-hinge kinking category as described by Ramsay (1974) and Stewart & Alvarez (1991). This structure coincides particularly well with lattice plane kinks observed in experimentally and naturally deformed minerals such as ice (Wilson *et al.* 1986), peridotites (Nicolas *et al.* 1973) and biotites (Wilson 1980). It has been shown that these minerals commonly develop sharp kinks along parallel slip planes (traces) after deformation (see Wilson *et al.* 1986, fig. 8). In particular, Nicolas *et al.* (1973) described kinks developed in deformed peridotites with kink boundaries normal to the flattening axis. These features are in good agreement with the kink–subgrain geometry developed in this study and are in support of the mechanism of kink formation presented. However, it should be pointed out that the wavelengths of kink–subgrain structures formed in some grains (e.g. grain (7,2) in Fig. 5c) are largely dependent on the finite difference mesh size. That is, they develop throughout a grain and their wavelength is based on the element size. These kink–subgrain structures may not precisely predict true kink geometries in grains.

Polycrystalline deformation

The initiation of inhomogeneous deformation is of critical importance in the process of deformation (Hobbs & Ord 1989, Hobbs *et al.* 1990). From the current deformation results, we can distinguish the origins of inter-grain and intra-grain inhomogeneous strains in polycrystals. Inter-grain inhomogeneous strain originates from contrasting deformation of neighbouring grains. Different grains have different lattice orientations and possess different deformabilities. Inter-grain strain inhomogeneity then must occur, particularly between 'soft' grains and 'hard' grains. In contrast, intra-grain inhomogeneous strain seems to be caused by the condition of strain compatibility between neighbouring grains. Strain compatibility requires that grain boundaries remain in contact after deformation, and thus strain transition from grain to grain is gradual (compatible). This means that the deformation of the boundary areas of any two neighbouring grains must be a compromise and be different from the deformations of their respective grain centres, so that strain across the boundary is compatible. As a result, strain within a grain varies from the central area to the boundary area and intra-grain strain inhomogeneity arises. The above discussion also suggests that inhomogeneous deformation is not always an obstacle to achieving strain compatibility; it is a two-fold effect. On the one hand, inter-grain strain inhomogeneity causes the compatibility problem. On the other hand, intra-grain strain inhomogeneity facilitates the maintenance of strain compatibility.

Because of the intra-grain inhomogeneous deformation caused by grain interaction at grain boundaries, the mesh size of single grains could have a certain influence on intra-grain strain and microstructure and the overall fabric pattern. Figure 14 gives the result of a pure shearing experiment started from a numerical specimen almost identical to the one shown in Fig. 2. The only difference is that the number of elements for a single grain was increased from 36 (6 × 6) to 100 (10 × 10). Comparing the new results (Fig. 14) with those of previous runs (Figs. 5c, 7c and 10c) shows that the basic fabric and deformation features of the previous experiments are retained. However, some fine intra-grain variations may be seen. These are most notably expressed as the smoother transition of slip-plane traces (microstructure) and strain within single grains from boundary to boundary [e.g. grains (1,6), (2,2), (2,7) and (6,5) in Fig. 14; cf. Figs. 5c and 10c]. This change arises obviously because more elements are available in a grain so that the partition between the boundary areas and interior area of a grain becomes larger. A further increase in the number of elements may further enhance the intra-grain features of polycrystalline deformation.

It is easy to understand the situations in which 'soft' grains are characterized by initial slip-plane orientations roughly parallel to the bulk shortening directions or parallel to the macroscopic shearing plane. This is because in both positions, slip planes are subjected to either an active kinking process or constant maximum

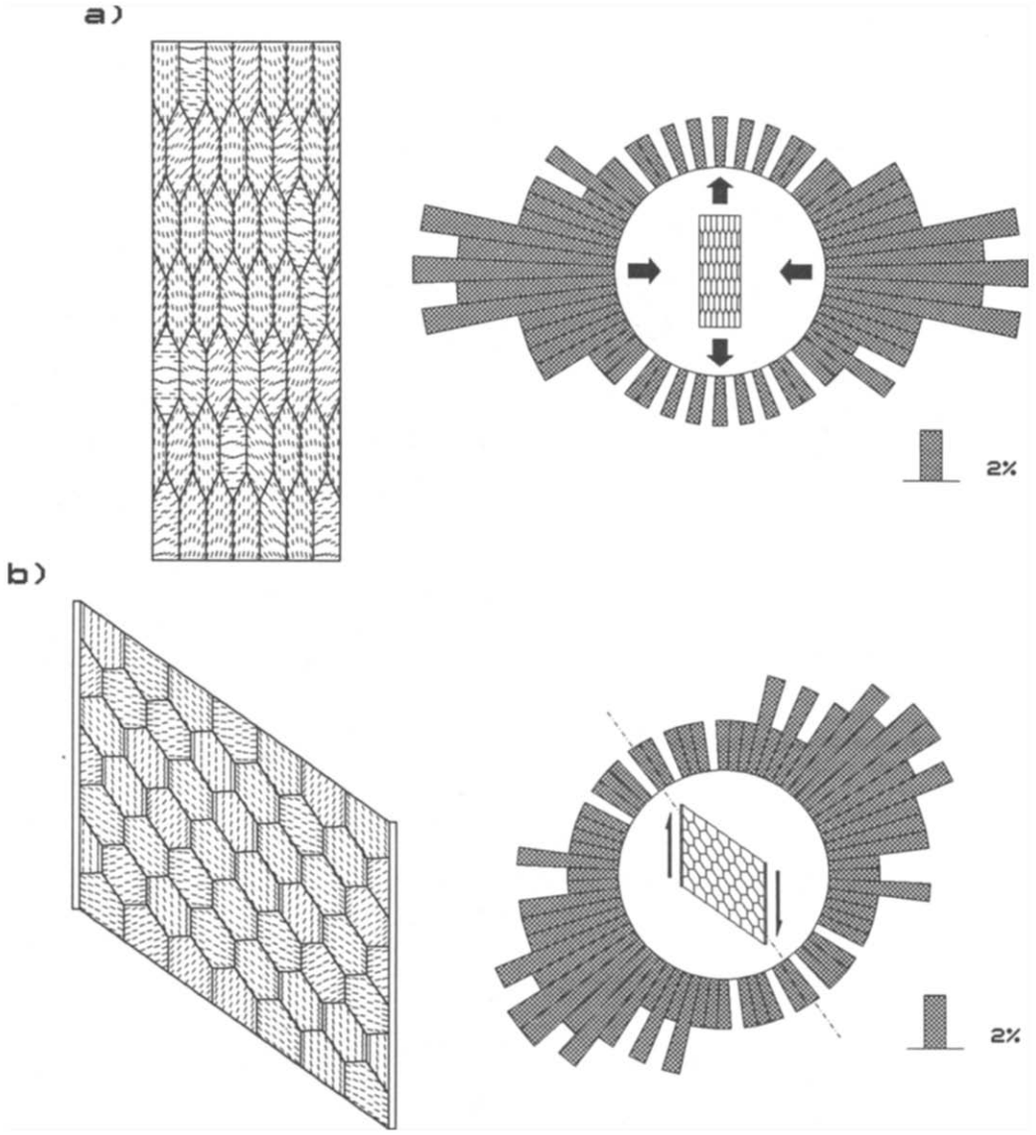

Fig. 13. Final 'passive' marker traces (left) and orientation distribution of marker normals (right). (a) Pure shearing, 38% bulk shortening; (b) simple shearing, $\gamma = 0.72$. See text for further explanation.

shearing. However, the situations in which 'soft' grains have initial slip-plane orientations oblique to the bulk shortening direction at about 30° (coaxial deformation) or 25° (simple shearing) rather than at 45° (maximum shear directions) are unexpected. An explanation is given here by taking slip-plane rotation into consideration. Obviously, in the process of deformation, slip planes initially parallel to the maximum shear directions will rotate away and toward more stable positions (Figs. 15a & b), whereas those initially oriented at about 30° (coaxial deformation) or 25° (simple shearing) to the bulk shortening directions will rotate toward and then pass the maximum shear directions (Figs. 15c & d). Therefore, for an average slip plane rotation (larger than 15° for coaxial deformation and 20° for simple shearing) the accumulated slip on slip planes is actually larger in the second situation than in the first. This explains why the grains with slip planes initially parallel to the maximum shear directions generally do not show the largest strain; however, the shearing plane in simple shearing is an exception because it is rotationally-stable.

An important feature of polycrystalline deformation revealed by this study is the highly inhomogeneous distribution of strain and stress. This seems to suggest that the current model better applies to the low-temperature deformation of real materials, where strain localization is a common phenomenon. In addition, the model should be particularly relevant to the deformation of minerals in which the major deformation mechanism is dislocation glide on limited slip systems, such as ice (Burg *et al.* 1986), biotite (Wilson 1980) and peridotites (Nicolas *et al.* 1973). In high-temperature and low-strain rate situations, other creep mechanisms (e.g. diffusion creep) are generally believed to be im-

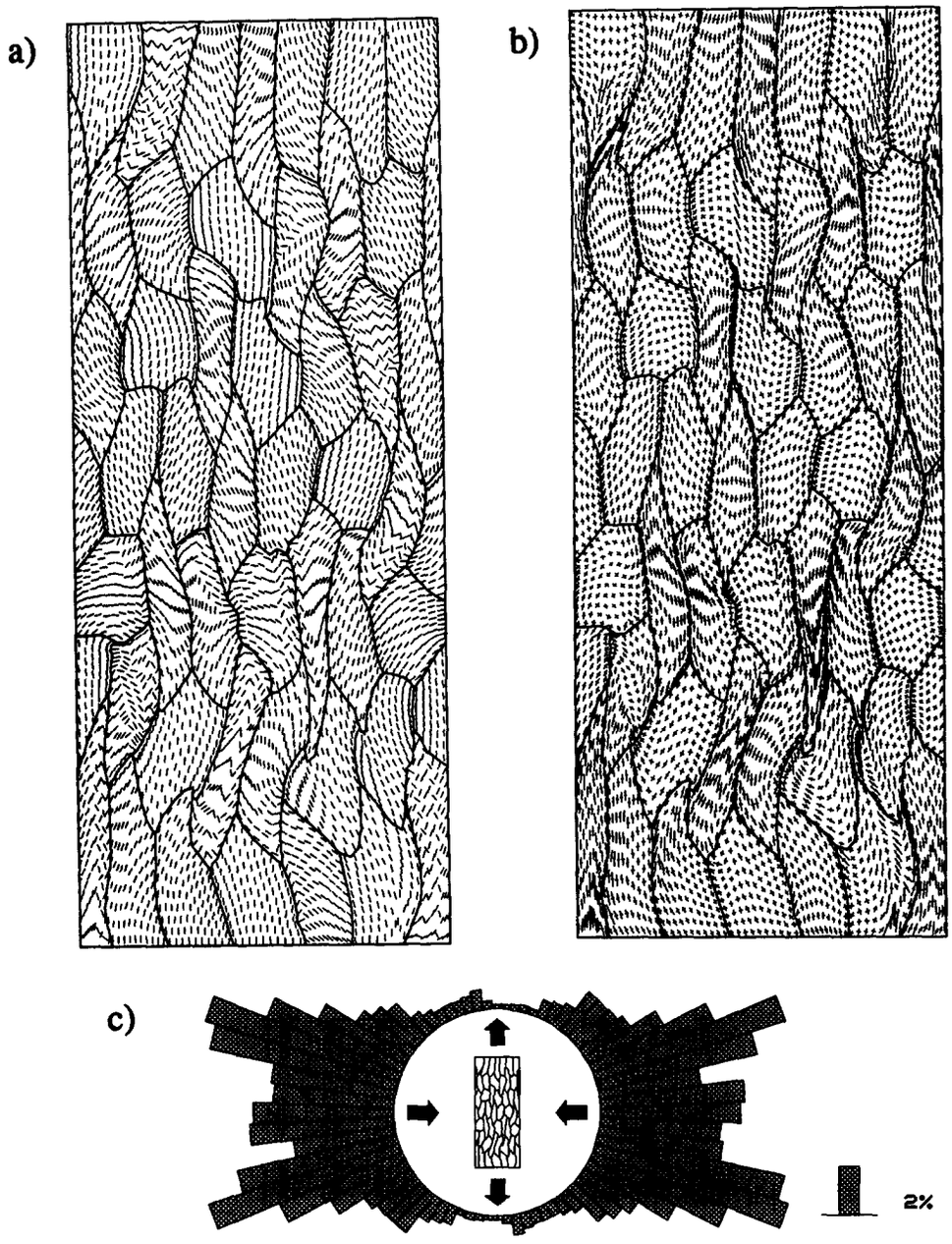

Fig. 14. The spatial distribution of (a) slip-plane traces and (b) strain ellipse axes, and (c) the preferred orientation of slip-plane normals at the 37% bulk shortening level for a pure shearing experiment involving a large mesh size. The starting configuration is similar to that shown in Fig. 2, but the number of elements in a single grain is increased from 36 to 1200 (see text for further explanation).

portant (Ranalli 1987). The strain distribution could then become quite homogeneous. The results of this model may not apply to such situations.

CONCLUSIONS

(1) Strain and stress are inhomogeneous on both the intra-grain and inter-grain scales. Intra-grain inhomogeneity originates from the constraint of strain compatibility. Conversely, strain compatibility is only possible when intra-grain inhomogeneous strain is allowed. Different grains show different deformabilities, dominantly depending on the corresponding initial slip-plane orientations. The end-members are defined as 'hard' grains and 'soft' grains. The contrasting deformability of neighbouring grains is the origin of inter-grain strain inhomogeneity.

(2) Various microstructures are developed, including flattened grains, local shear zones, subgrains, kink–subgrain structures and undulatory lattice orientations. Kink–subgrain structures only develop in the grains with slip-plane orientations initially subparallel to the bulk shortening direction.

(3) The preferred orientations of slip planes do not coincide with the preferred alignment of long axes of deformed grains. The former varies according to deformation history, while the latter is always parallel to the bulk extension direction.

(4) The rotationally stable positions for slip planes differ from those for passive plates in a deforming ductile medium.

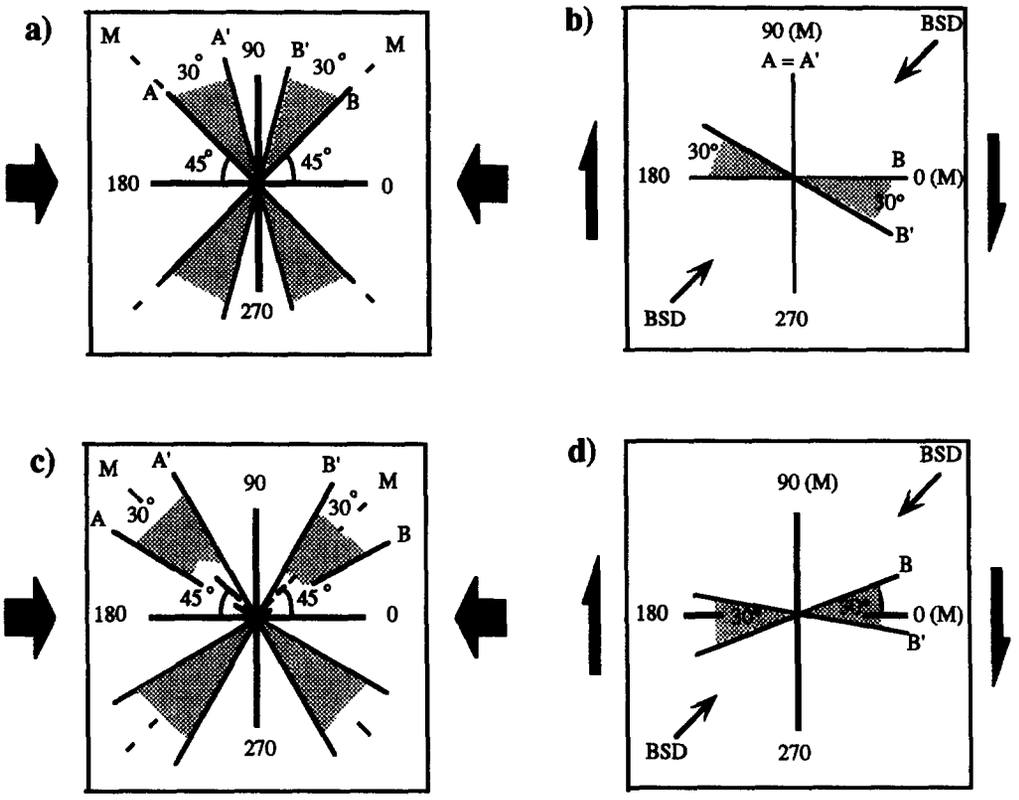

Fig. 15. Sketch of possible slip-plane rotations during coaxial shortening (a & c) and simple shearing (b & d). M, the maximum shearing direction; BSD, the bulk shortening direction; A and B, initial positions of slip planes; A' and B', the final positions of the slip planes. See text for further explanation.

Acknowledgements—We would like to thank Peter Hudleston and two anonymous reviewers for their helpful comments and suggestions, by which the manuscript has been greatly improved. M. W. Jessell and W. D. Means are also thanked for their help in the early stages of the work.

REFERENCES

Bishop, J. F. W. & Hill, R. 1951. A theory of plastic distortion of a polycrystalline aggregate under combined stresses. *Phil. Mag.* **42**, 414–427.

Board, M. 1989. *FLAC*: Fast Lagrangian Analysis of Continua, User Manual, Version 2.20, Software Summary. Itasca Consulting Group, Inc., Minneapolis.

Bouchez, J. L. & Duval, P. 1982. The fabric of polycrystalline ice deformed in simple shear: experiments in torsion, natural deformation and geometric interpretation. *Textures & Microstruct.* **5**, 171–190.

Burg, J. P., Wilson, C. J. L. & Mitchell, J. C. 1986. Dynamic recrystallization and fabric development during the simple shear deformation of ice. *J. Struct. Geol.* **8**, 857–870.

Clark, S. P., Jr (editor) 1966. *Handbook of Physical Constants. Mem. geol. Soc. Am.* **97**.

Cundall, P. A. 1989. Numerical experiments on localization in frictional materials. *Ingenieur-Archiv.* **59**, 148–159.

Cundall, P. A. 1990. Numerical modelling of jointed and faulted rock. In: *Proc. Int. Conf. on Mechanics of Jointed and Faulted Rock*, 11–18.

Cundall, P. A. & Board, M. 1988. A microcomputer program for modelling large-strain plasticity problem. In: *Numerical Methods in Geomechanics* (edited by Swobada, C.). *Proc.* 6th *Int. Conf. on Numerical Methods in Geomechanics*. Balkema, Rotterdam, 2101–2108.

Etchecopar, A. 1977. A plane kinematic model of progressive deformation in a polycrystalline aggregate. *Tectonophysics* **39**, 121–139.

Etchecopar, A. & Vasseur, G. 1987. A 3-D kinematic model of fabric development in polycrystalline aggregates: Comparisons with experimental and natural examples. *J. Struct. Geol.* **9**, 705–717.

Harren, S. V. & Asaro, R. J. 1989. Nonuniform deformation in polycrystals and aspects of the validity of the Taylor model. *J. Mech. Phys. Solids* **37**, 191–233.

Hobbs, B. E., Mühlhaus, H.-B. & Ord, A. 1990. Instability, softening and localization of deformation. In: *Deformation Mechanisms, Rheology and Tectonics* (edited by Knipe, R. J. & Rutter, E. H.). *Spec. Publs geol. Soc. Lond.* **54**, 143–165.

Hobbs, B. E. & Ord, A. 1989. Numerical simulation of shear band formation in a frictional-dilational material. *Ingenieur-Archiv.* **59**, 209–220.

Honneff, H. & Mecking, H. 1978. A method for the determination of the active slip systems and orientation changes during single crystal deformation. In: *Proc.* 5th *Int. Conf. on Texture of Materials* (edited by Gottstein, G. & Lücke, K.). Springer, New York, 265–275.

Honneff, H. & Mecking, H. 1981. Analysis of the deformation texture at different rolling conditions. In: *Proc.* 6th *Conf. on Texture of Materials*. The Iron and Steel Institute of Japan, Tokyo, 347–355.

Hudleston, P. J. 1980. The progressive development of inhomogeneous shear and crystallographic fabric in glacial ice. *J. Struct. Geol.* **2**, 189–196.

Jessell, M. W. 1988a. Simulation of fabric development in recrystallizing aggregates—I. Description of the model. *J. Struct. Geol.* **10**, 771–778.

Jessell, M. W. 1988b. Simulation of fabric development in recrystallizing aggregates—II. Example model runs. *J. Struct. Geol.* **10**, 779–793.

Jessell, M. W. & Lister, G. S. 1990. A simulation of the temperature dependence of quartz fabrics. In: *Deformation Mechanisms, Rheology and Tectonics* (edited by Knipe, R. J. & Rutter, E. H.). *Spec. Publs geol. Soc. Lond.* **54**, 353–362.

Kocks, U. F. & Canova, G. R. 1981. How many slip systems and which? In: *Deformation of Polycrystals: Mechanisms and Microstructures, Proc.* 2nd *RISO Int. Symp.*, Riso National Laboratory, Roskilde, Denmark, 35–44.

Lister, G. S. & Hobbs, B. E. 1980. The simulation of fabric development during plastic deformation and its application to quartzite: the influence of deformation history. *J. Struct. Geol.* **2**, 355–370.

Lister, G. S. & Paterson, M. S. 1979. The simulation of fabric development during plastic deformation and its application to quartzite: Fabric transitions. *J. Struct. Geol.* **1**, 99–115.

Lister, G. S., Paterson, M. S. & Hobbs, B. E. 1978. The simulation of

fabric development during plastic deformation and its application to quartzite: the model. *Tectonophysics* **45**, 107–158.
Means, W. D. & Ree, J. H. 1988. Seven types of subgrain boundaries in octachloropropane. *J. Struct. Geol.* **10**, 765–770.
Molinari, A., Canava, G. R. & Ahzi, S. 1987. A self-consistent approach of the large deformation polycrystal viscoplasticity. *Acta metall.* **35**, 2983–2994.
Nakaya, U. 1954. The deformation of single crystals of ice. *J. Glaciol.* **2**, 229–240.
Nicolas, A., Boudier, F. & Boullier, A. M. 1973. Mechanisms of flow in naturally and experimentally deformed peridotites. *Am. J. Sci.* **273**, 853–876.
Nicolas, A. & Poirier, J. P. 1976. *Crystalline Plasticity and Solid-state Flow in Metamorphic rocks*. Wiley, New York.
Ord, A. 1990. Mechanical controls on dilatant shear zones. In: *Deformation Mechanisms, Rheology and Tectonics* (edited by Knipe, R. J. & Rutter, E. H.). *Spec. Publs geol. Soc. Lond.* **54**, 183–192.
Price, C.-P. 1985. Preferred orientations in quartzites. In: *Preferred Orientations in Deformed Metals and Rocks* (edited by Wenk, H.-R.). Academic Press, London, 385–406.
Ramsay, J. G. 1974. Development of chevron folds. *Bull geol. Soc. Am.* **85**, 1741–1754.
Ranalli, G. 1987. *Rheology of the Earth*. Allen & Unwin, London.
Ree. J.-H. 1990. High temperature deformation of octachloropropane: dynamic grain growth and lattice reorientation. In: *Deformation Mechanisms, Rheology and Tectonics* (edited by Knipe, R. J. & Rutter, E. H.). *Spec. Publs geol. Soc. Lond.* **54**, 363–368.
Steward, K. G. & Alvarez, W. 1991. Mobile-hinge kinking in layered rocks and models. *J. Struct. Geol.* **13**, 243–259.
Taylor, G. I. 1938. Plastic strain in metals. *J. Inst. Metals* **62**, 307–324.
Tharp, T. M. 1989. Crystal rotation by mechanical interaction between plastically anisotropic crystals. *J. Struct. Geol.* **11**, 613–623.
Tullis, J. A., Christie, J. M. & Griggs, D. T. 1973. Microstructures and preferred orientations of experimentally deformed quartzites. *Bull. geol. Soc. Am.* **84**, 294–314.
Wenk, H.-R., Bennett, K., Canova, G. & Molinari, A. 1991. Modelling plastic deformation of peridotite with the self-consistent theory. *J. geophys. Res.* **96B**, 8337–8349.
Wenk, H.-R., Canovar, G., Molinari, A. & Kocks, U. F. 1989a. Viscoplastic modelling of texture development in quartzite. *J. geophys. Res.* **94B**, 17,895–17,906.
Wenk, H.-R., Canova, G., Molinari, A. & Mecking, H. 1989b. Texture development in halite: comparison of Taylor model and self-consistent theory. *Acta metall.* **37**, 2017–2029.
Wenk, H.-R. & Christie, J. M. 1991. Comments on the interpretation of deformation textures in rocks. *J. Struct. Geol.* **13**, 1091–1110.
Wilson, C. J. L. 1980. Shear zones in a pegmatite: a study of albite–mica–quartz deformation. *J. Struct. Geol.* **2**, 203–209.
Wilson, C. J. L. 1982. Fabrics in polycrystalline ice deformed experimentally at −10°C. *Cold Regions Sci. & Technol.* **6**, 149–161.
Wilson, C. J. L., Burg, J. P. & Mitchell, J. C. 1986. The origin of kinks in polycrystalline ice. *Tectonophysics* **127**, 27–48.
Zhang, Y., Hobbs, B. E. & Jessell M. W. 1993. Crystallographic preferred orientation development in a buckled single layer: A computer simulation. *J. Struct. Geol.* **15**, 265–276.